4896 *Inorg. Chem.* **2009,** *48,* 4896–4907
DOI:10.1021/ic900295n

Inorganic Chemistry
Article

Photochemically-Induced Acid Generation from 18-Molybdodiphosphate and 18-Tungstodiphosphate within Poly(2-Hydroxyethyl Methacrylate) Films

Antonios M. Douvas,*,† Anna Kapella,†,‡ Dimitra Dimotikali,‡ and Panagiotis Argitis*,†

†*Institute of Microelectronics, National Center for Scientific Research "Demokritos", 15310 Aghia Paraskevi, Athens, Greece and* ‡*Department of Chemical Engineering, National Technical University of Athens, 15780 Zographou, Athens, Greece*

Received February 12, 2009

The capability of ammonium 18-molybdodiphosphate, $(NH_4)_6P_2Mo_{18}O_{62}$ (Mo_{18}^{6-}), and ammonium 18-tungstodiphosphate, $(NH_4)_6P_2W_{18}O_{62}$ (W_{18}^{6-}), to photochemically generate acid within films of a polymer with hydroxylic functional groups (namely, within poly(2-hydroxyethyl methacrylate) (PHEMA) films) is demonstrated. Upon UV irradiation, both 2:18 polyoxometalates (POMs) investigated are reduced with concomitant oxidation of PHEMA and generation of acid, which subsequently catalyzes the cross-linking of PHEMA. The photoacid generation is mainly evidenced by monitoring the protonation of an appropriate acid indicator (4-dimethylamino-4′-nitrostilbene) with UV spectroscopy and by photolithographic imaging experiments. By comparing the efficiency of both POMs to induce acid-catalyzed cross-linking of PHEMA under similar conditions, the W_{18}^{6-} ion is found to be more efficient in photoacid generation than the Mo_{18}^{6-} ion. Imaging of the POM-containing PHEMA films through UV photolithographic processing is demonstrated. In that process, both POMs can be entirely leached during the development step by using pure water as a developer, resulting in patterned PHEMA films. This characteristic renders the investigated POMs attractive materials for applications, especially in the area of biomaterials, where removal of the photoacid generator from the film at the end of the process is desirable.

Introduction

In the past decade, a new boost has been given to the already well-developed area of polyoxometalate (POM) chemistry, mainly due to progress in the crystallographic characterization techniques[1,2] and to theoretical investigations.[3] Meanwhile, new interdisciplinary areas of research have emerged exploiting the unique structural, reactivity, and electronic properties of POMs.[1,4,5] In general, POMs constitute a large category of polynuclear metal−oxygen anionic clusters with well-defined structures.[1,6−8] They are characterized by controllable oxidizing efficiency, a property that stems from their ability to accept (in a stepwise and chemically reverse way) a certain number of electrons without substantial alteration of their structure.[6−8] By absorbing UV or near-visible light, POMs become effective oxidizing reagents that are capable of oxidizing a broad variety of organic compounds,[9] including even the hardly oxidized hydrocarbons.[10] In addition, POMs are very weak bases (due to their particularly low surface charge density), and therefore, their conjugate acids (the heteropoly acids) are very strong acids, having a Brönsted acidity that approaches the super acid region.[11] Thus, POMs find applications in fields of high industrial and academic interest that are usually based either on the redox properties of POMs (e.g., in oxidation catalysis,[11,12] elemental analysis,[13] and solid-state electronic devices[14]) or on the high Brönsted

*To whom correspondence should be addressed. Phone: +30-210-6503231 (A.M.D.), +30-210-6503114 (P.A.). Fax: +30-210-6511723. E-mail: adouvas@imel.demokritos.gr (A.M.D.), argitis@imel.demokritos.gr (P.A.).

(1) Long, D.-L.; Burkholder, E.; Cronin, L. *Chem. Soc. Rev.* **2007**, *36*, 105.
(2) Müller, A.; Beckmann, E.; Bögge, H.; Schmidtmann, M.; Dress, A. *Angew. Chem., Int. Ed.* **2002**, *41*, 1162.
(3) (a) Poblet, J. M.; López, X.; Bo, C. *Chem. Soc. Rev.* **2003**, *32*, 297. (b) López, X.; Bo, C.; Poblet, J. M.; Sarasa, J. P. *Inorg. Chem.* **2003**, *42*, 2634.
(4) Lehmann, J.; Gaita-Arino, A.; Coronado, E.; Loss, D. *Nat. Nanotechnol.* **2007**, *2*, 312.
(5) Kapetanakis, E.; Douvas, A. M.; Velessiotis, D.; Makarona, E.; Argitis, P.; Glezos, N.; Normand, P. *Adv. Mater.* **2008**, *20*, 1.
(6) (a) Pope, M. T.; Müller, A. *Angew. Chem., Int. Ed. Engl.* **1991**, *30*, 34. bPope, M. T. *Heteropoly and Isopoly Oxometalates*; Springer-Verlag: Berlin, 1983.
(7) Papaconstantinou, E. *Chem. Soc. Rev.* **1989**, *18*, 1.
(8) Hiskia, A.; Mylonas, A.; Papaconstantinou, E. *Chem. Soc. Rev.* **2001**, *30*, 62.
(9) Hiskia, A.; Papaconstantinou, E. *Inorg. Chem.* **1992**, *31*, 163.
(10) Renneke, R. F.; Hill, C. L. *J. Am. Chem. Soc.* **1986**, *108*, 3528.
(11) (a) Kozhevnikov, I. V. *Chem. Rev.* **1998**, *98*, 171. (b) Drago, R. S.; Dias, J. A.; Maier, T. O. *J. Am. Chem. Soc.* **1997**, *119*, 7702.
(12) Misono, M.; Nojiri, N. *Appl. Catal.* **1990**, *64*, 1.
(13) Katsoulis, D. E. *Chem. Rev.* **1998**, *98*, 359.
(14) (a) Douvas, A. M.; Makarona, E.; Glezos, N.; Argitis, P.; Mielczarski, J. A.; Mielczarski, E. *ACS Nano* **2008**, *2*, 733. (b) Makarona, E.; Kapetanakis, E.; Velessiotis, D. M.; Douvas, A.; Argitis, P.; Normand, P.; Gotszalk, T.; Woszczyna, M.; Glezos, N. *Microelectron. Eng.* **2008**, *85*, 1399. (c) Glezos, N.; Argitis, P.; Velessiotis, D.; Diakoumakos, C. D. *Appl. Phys. Lett.* **2003**, *83*, 488.

Published on Web 4/30/2009

acidity of their conjugate acids (e.g., in acid catalysis,[11,12] fuel cells,[15] and proton memory devices[5]).

In the present paper, we investigate the combination of two major POM characteristics, that is, their photooxidizing efficiency and the low Brönsted basicity, and their possible use to photochemically generate acid within a polymer matrix that includes suitable functional groups. The generation of protons is expected through the POM photoreduction and the subsequent oxidation of a hydroxylic group according to a generally accepted mechanism for the photocatalytic oxidation of alcohols by POMs in solution.[7] Due to the low Brönsted basicity of POMs, the protons are expected to be available for acid-catalyzed reactions within the polymer matrix. The acid generation is of high practical importance for a wide variety of applications in organic films. In particular, the photochemically induced acid generation is mainly employed in applications such as curing of coatings,[16] printing inks,[17] and numerous photolithographic processes both in mainstream semiconductor manufacturing[18] and in new emerging applications.[19] The photoacid generators (PAGs) used in those processes are usually sulfonium or iodonium salts, which are photolyzed upon UV or near-visible irradiation, generating an extremely strong Brönsted acid.[20] In most cases, the acid photogenerated by the onium salts is a super acid, such as, for example, the hexafluoroantimonic acid ($H^+SbF_6^-$) produced by the UV irradiation of triphenylsulfonium hexafluoroantimonate (TPSHFA).[20,21]

The POMs studied as possible photoacid generators in the present work are the ammonium 18-molybdodiphosphate ($(NH_4)_6P_2Mo_{18}O_{62}$ (Mo_{18}^{6-})) and the ammonium 18-tungstodiphosphate ($(NH_4)_6P_2W_{18}O_{62}$ (W_{18}^{6-})). The ammonium salts of two Dawson-type POMs were selected, because they are soluble in common organic solvents and are more stable in organic nonacidified matrices (because they are generally more stable at higher pH values) compared with the corresponding Keggin-type anions.[22] The study is carried out within films of polymers that comprise hydroxylic functional groups. Emphasis is given in the photoacid generation to poly (2-hydroxyethyl methacrylate (PHEMA) films. Upon UV irradiation, both 2:18 POMs investigated generate acid with concomitant oxidation of PHEMA, where the generated acid catalyzes next the cross-linking of PHEMA. The photogeneration of acid by both 2:18 POMs within the PHEMA films is also evidenced by UV monitoring of an appropriate acid indicator (4-dimethylamino-4′-nitrostilbene, DANS). The acid-induced cross-linking of PHEMA is studied, and imaging possibilities are discussed.

(15) Kim, W. B.; Voitl, T.; Rodriguez-Rivera, G. J.; Dumesic, J. A. *Science* **2004**, *305*, 1280.
(16) Shirai, M. *Prog. Org. Coat.* **2007**, *58*, 158.
(17) Crivello, J. V. *J. Photopol. Sci. Tech.* **2008**, *21*, 493.
(18) (a) Wallraff, G. M.; Hinsberg, W. D. *Chem. Rev.* **1999**, *99*, 1801. (b) Reichmanis, E.; Houlihan, F. M.; Nalamasu, O.; Neenan, T. X. *Chem. Mater.* **1991**, *3*, 394.
(19) (a) Vasilopoulou, M.; Georgiadou, D.; Pistolis, G.; Argitis, P. *Adv. Funct. Mater.* **2007**, *17*, 3477. (b) Pan, F.; Wang, P.; Lee, K.; Wu, A.; Turro, N. J.; Koberstein, J. T. *Langmuir* **2005**, *21*, 3605. (c) Douvas, A.; Argitis, P.; Misiakos, K.; Dimotikali, D.; Petrou, P. S.; Kakabakos, S. E. *Biosens. Bioelectron.* **2002**, *17*, 269.
(20) Dektar, J. L.; Hacker, N. P. *J. Am. Chem. Soc.* **1990**, *112*, 6004.
(21) March, J. *Advanced Organic Chemistry: Reactions, Mechanisms and Structures*, 4th ed.; Wiley-Interscience: New York, 1992.
(22) (a) Briand, L. E.; Baronetti, G. T.; Thomas, H. J. *Appl. Catal., A* **2003**, *256*, 37. (b) Song, I. K.; Barteau, M. A. *J. Mol. Catal. A* **2004**, *212*, 229.

Experimental Section

Materials. Two 2:18 POMs (both α isomers), namely, the ammonium 18-molybdodiphosphate, α-$(NH_4)_6P_2Mo_{18}O_{62}\cdot xH_2O$ (Mo_{18}^{6-}), and the ammonium 18-tungstodiphosphate, α-$(NH_4)_6P_2W_{18}O_{62}\cdot xH_2O$ (W_{18}^{6-}), were synthesized according to well-established methods.[23] 12-Tungstophosphoric acid hydrate $H_3PW_{12}O_{40}\cdot xH_2O$ (obtained from Aldrich), triphenylsulfonium hexafluoroantimonate ($Ph_3S^+SbF_6^-$; TPSHFA; obtained from Midori Kagakou), and 4-dimethylamino-4′-nitrostilbene (DANS; obtained from Fluka) were of analytical grade and used without further purification. The homopolymers, poly(2-hydroxyethyl methacrylate) (PHEMA; MW 300 000; purchased from Aldrich) and poly(vinyl alcohol) (PVA; MW 13 000−23 000; 98% hydrolyzed; obtained from Aldrich), were used as received. The solvents, methanol, ethyl lactate (EL), *N,N*-dimethylformamide (DMF) (all obtained from Aldrich), were also of analytical grade. Deionized water with a resistivity of 15 MΩ cm^{-1} prepared from the Milli-RO plus 90 apparatus (Millipore) was used where necessary.

Characterization Methods. UV−vis absorption spectra were obtained on quartz slides using a Perkin-Elmer UV−vis Lambda 40 spectrophotometer. FTIR transmittance spectra at 4 cm^{-1} resolution and 128 scans were recorded on silicon wafers using a Bruker Tensor 27 spectrometer. The thickness of the polymeric films was measured using an Ambios technology XP-2 profilometer. Scanning electron microscopy (SEM) micrographs of the photolithographic patterns were obtained on a LEO 440 Zeiss-Leica SEM instrument.

Polymeric Film Preparation and Lithographic Processing. Solutions of PVA (4.4% w/w in water) and PHEMA (6.3% w/w in EL; 3.5−4.7% w/w in a methanol/water mixture (at a weight ratio ranging from 0.7:1 to 1.3:1); 30% w/w in DMF) were prepared. The concentrated PHEMA solutions (30% w/w in DMF) were used only in the monitoring of the photoacid generation within the PHEMA films (i.e., when the acid indicator, DANS, was used). The high PHEMA concentration was necessary because, when low-concentrated PHEMA formulations containing the DANS indicator were used, a significantly high concentration of indicator was removed from the film during the spin coating. In some of the PVA and PHEMA solutions, one of the following compounds, Mo_{18}^{6-} (1.18−76.6% w/w in solids), W_{18}^{6-} (1.18−40.4% w/w in solids), TPSHFA (0.13% w/w in solids), or $H_3PW_{12}O_{40}$ (0.08% w/w in solids), was added. In some of the resulted solutions, DANS (at a molar ratio of Mo_{18}^{6-}, W_{18}^{6-}, or TPSHFA to DANS of 1:1 or at a molar ratio of $H_3PW_{12}O_{40}$ to DANS ranging from 1:10 to 5:1) was added.

In a typical film preparation process, the POM-containing polymeric films were spin-coated (at 500−3000 rpm) onto silicon wafers. The films formed (100−300 nm thick) were thermally treated at 50−90 °C, for 2−10 min, during a post apply bake (PAB) step. Then, the films were exposed to deep UV light (using a DUV Orial Hg−Xe, 500 W exposure tool) in three alternative ways: (a) through a 248 nm narrow-band (7 nm bandwidth at half-maximum) filter, (b) through a 254 nm broad-band (50 nm bandwidth at half-maximum) filter, and (c) without a filter (wavelength range, 220−280 nm), when high exposure doses were necessary. In the photolithographic process, the POM-containing polymeric films were exposed only through the 248 nm narrow-band filter, in a contact-printing mode. Also, in the latter process, further steps followed after the exposure. In particular, the polymeric films were thermally treated at 80−90 °C, for 2−5 min, during a post exposure bake (PEB) step. Finally, a development step followed, in which the films were developed in deioized water (except for a few cases in EL).

(23) Wu, H. *J. Biol. Chem.* **1920**, *43*, 189.

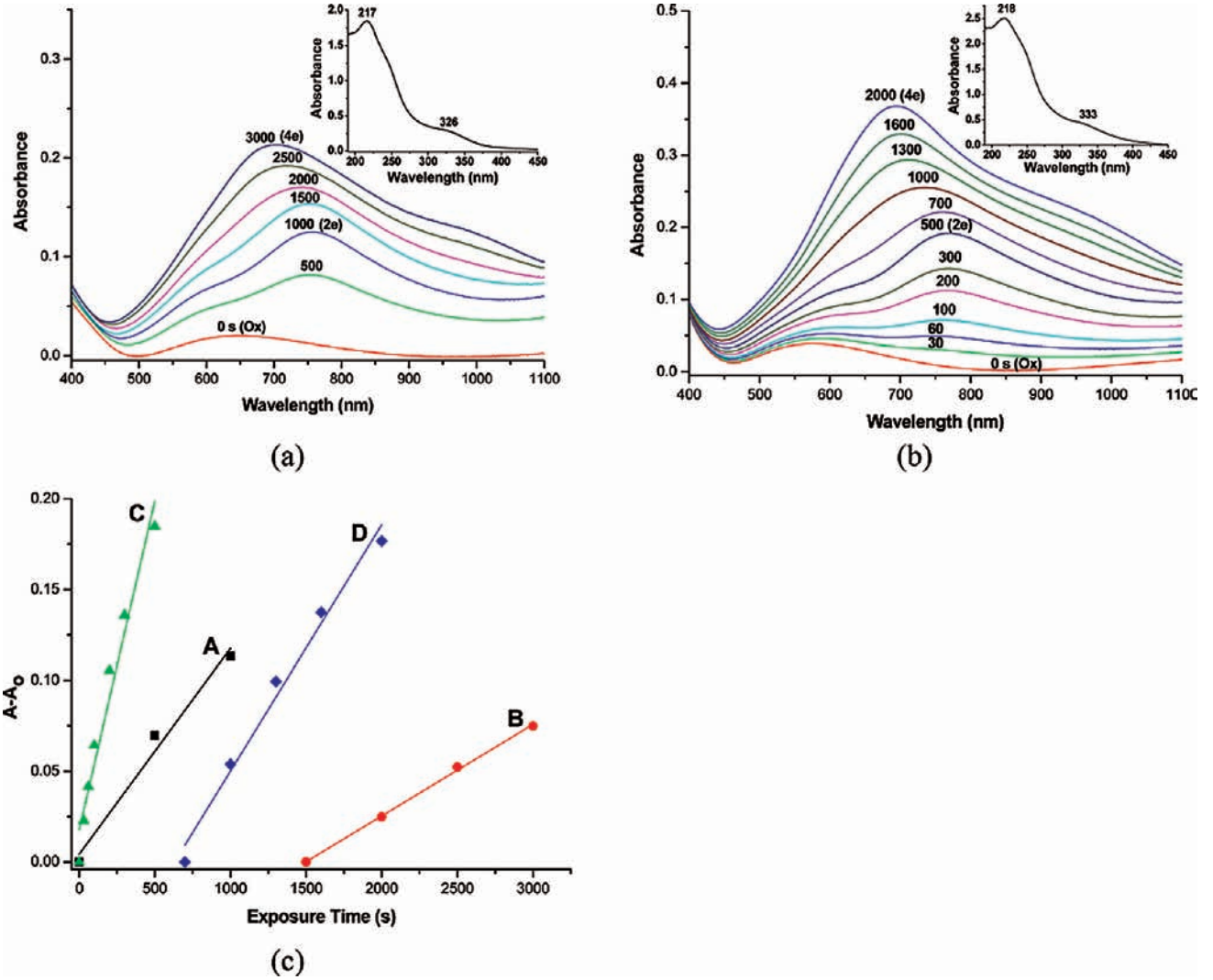

Figure 1. UV monitoring of the photoreduction of the Mo_{18}^{6-} ions within (a) a PHEMA film and (b) a PVA film. The exposure times (s) are indicated on the spectra. Inset (a): The initial UV spectrum of the Mo_{18}^{6-} ions within the PHEMA film. Inset (b): The initial UV spectrum of the Mo_{18}^{6-} ions within the PVA film. (c) Change of the absorption intensity of two IVCT bands of the Mo_{18}^{6-} ions with the exposure time. Curves A and B correspond to the $2e^-$ and $4e^-$ photoreduction of the Mo_{18}^{6-} ions (IVCT peaks at 759 and 702 nm, respectively) within a PHEMA film. Curves C and D correspond to the $2e^-$ and $4e^-$ photoreduction of the Mo_{18}^{6-} ions (IVCT peaks at 768 and 695 nm, respectively) within a PVA film. The assignments Ox, $2e^-$, and $4e^-$ represent the oxidized state and the two-electron and four-electron reduced states of the Mo_{18}^{6-} ions, respectively. The process conditions are described in ref 41.

Results and Discussion

1. POM Photoreduction in Polymer Matrices with Hydroxylic Functional Groups. a. Monitoring of Mo_{18}^{6-} Photoreduction with UV Spectroscopy. The photoreduction of the Mo_{18}^{6-} ions is studied within two polymer matrices that include hydroxylic functional groups, that is, within PHEMA and PVA films, where the study in the PVA films is conducted mainly for comparison reasons. In the past, the photoreduction of 12-tungstophosphoric acid ($H_3PW_{12}O_{40}$) within PVA films has been studied, where photooxidation of PVA and subsequent Diels–Alder cross-linking took place selectively in the exposed film areas forming the basis for a deep UV photoresist.[24] In the present study, it was first proved that the Mo_{18}^{6-} ions are photoreduced within a PHEMA film through the successive addition of two and four electrons (Figure 1a, Table 1a). The photoreduction of the Mo_{18}^{6-} ions is easily monitored with UV spectroscopy, because their reduced ions are practically not reoxidized by oxygen, and characteristic absorption bands are formed during that process.[7,9,25] Upon broad-band DUV (wavelength range 220−280 nm) irradiation of their oxygen-to-metal charge transfer (OMCT: O → Mo; Figure 1a inset) bands, the Mo_{18}^{6-} ions are progressively reduced with two electrons, as shown from the gradual increase of their intervalence charge transfer (IVCT: $Mo^V \rightarrow Mo^{VI}$) band at ~759 nm. It is assumed that almost all of the Mo_{18}^{6-} ions are converted to the two-electron heteropoly blues, Mo_{18}^{8-} ions, when the IVCT band is located at 759 nm (i.e., after 1000 s exposure time).[26] Subsequently, by increasing the exposure time, the Mo_{18}^{8-} ions formed are further reduced with two electrons, as depicted by the further increase and shift of the IVCT band at lower wavelengths (Figure 1a). Approximately all of the Mo_{18}^{8-} ions are converted to the four-electron heteropoly blues, Mo_{18}^{10-} ions, when the

(24) Carls, J. C.; Argitis, P.; Heller, A. *J. Electrochem. Soc.* **1992**, *139*, 786.

(25) Papaconstantinou, E.; Dimotikali, D.; Politou, A. *Inorg. Chim. Acta* **1980**, *46*, 155.

(26) Papaconstantinou, E.; Pope, M. T. *Inorg. Chem.* **1970**, *9*, 667.

Table 1. (a) UV and FTIR Bands of the Mo_{18}^{6-} Ions during Their Photoreduction within Both PHEMA and PVA films and (b) UV and FTIR Bands of the W_{18}^{6-} Ions within PHEMA films (the process conditions are described in ref [40])

(a) Mo_{18}^{6-}			UV bands (nm)[a]		FTIR bands (cm^{-1})[b]			
polymer matrix	redox state	ET (s)[c]	OMCT (O → Mo)	IVCT ($Mo^{V} \rightarrow Mo^{VI}$)	ν_{as} (P−O_a)	ν_{as} (Mo=O_d)	ν_{as} (Mo−O_b−Mo)	ν_{as} (Mo−O_c−Mo)
PHEMA	Ox[d]	0	217[e], 326[e]		1078, 1003	941	905	835, 783
	2e[f]	1000		759	1078, 1003	941	905	835, 782
	4e[g]	3000		702, 976[e]	1079, 1003	944	904	834, 782
PVA	Ox	0	218[e], 333[e]		1079, 1003	940	906	832, 779
	2e	500		768	1078, 1003	939	904	832, 784
	4e	2000		695, 970[e]	1081, 1004	940	905	836, 787

(b) W_{18}^{6-}			UV bands (nm)[h]		FTIR bands (cm^{-1})[i]			
polymer matrix	redox state	ET (s)	OMCT (O→W)	IVCT ($W^{V} \rightarrow W^{VI}$)	ν_{as} (P−O_a)	ν_{as} (W=O_d)	ν_{as} (W−O_b−W)	ν_{as} (W−O_c−W)
PHEMA	Ox[j]	0	258[e], 312[e]		1090, 1022	960	909	795

[a] Assignment based on ref 26. [b] Assignment based on ref 29. [c] Exposure time (s) at broadband DUV (220−280 nm) irradiation. [d] Oxidized state of Mo_{18}^{6-} ions (Mo_{18}^{6-}). [e] Shoulder. [f] Two-electron reduced state of Mo_{18}^{6-} ions (Mo_{18}^{8-}). [g] Four-electron reduced state of Mo_{18}^{6-} ions (Mo_{18}^{10-}). [h] Assignment based on ref 33. [i] Assignment based on ref 34. [j] Oxidized state of W_{18}^{6-} ions (W_{18}^{6-}).

position of the IVCT band is at ~702 nm (actually, there are two IVCT bands, but the second one is a shoulder at ~976 nm).[26] The stepwise photoreduction of the Mo_{18}^{6-} ions within the PHEMA film is in good agreement with previous findings reporting the photoreduction of those ions in aqueous solutions of isopropyl alcohol.[7,22,25] Also, the OMCT bands of the Mo_{18}^{6-} ions embedded within the PHEMA film are considerably shifted (~14 nm) in relation to the corresponding bands of those ions dissolved in acidified aqueous solutions, as the OMCT bands are known to be sensitive to the solvent effect.[27]

The photoreduction of the Mo_{18}^{6-} ions within a PVA film proceeds with a way similar to the previous one within the PHEMA film (Figure 1b, Table 1a). The difference is that both the OMCT and IVCT bands of the Mo_{18}^{6-} ions within the PVA film are slightly shifted in comparison to the corresponding bands within the PHEMA film. In addition, lower exposure times for both the $2e^-$ and $4e^-$ photoreductions of the Mo_{18}^{6-} ions are necessary within the PVA film than those within the PHEMA film.

In order to have a clear picture about the photoreduction kinetics of the Mo_{18}^{6-} ions within both the PHEMA and PVA films, the change of the absorption intensity of the IVCT bands (of the Mo_{18}^{6-} ions within those films) versus the exposure time is studied (Figure 1c). Three major findings are extracted from that figure: (a) The absorption intensities of the IVCT bands vary linearly with the exposure time, indicating zero-order kinetics for both the $2e^-$ and $4e^-$ photoreductions of the Mo_{18}^{6-} ions within the PHEMA film (curves A and B, respectively, Figure 1c). The same holds true for the PVA film (curves C and D, respectively, Figure 1c). The zero-order kinetics of the photoreduction of the Mo_{18}^{6-} ions indicates that both concentrations of the excited $*Mo_{18}^{6-}$ ions and the polymer molecules are constant throughout the photoreduction (assuming that the initial Mo_{18}^{6-} ions absorb almost entirely the incident light). The concentration of the polymer molecules is considered practically constant during the photoreduction, because it is much higher than the concentration of the Mo_{18}^{6-} ions (initial molar ratios: Mo_{18}^{6-}/PHEMA, 1:17; Mo_{18}^{6-}/PVA, 1:20). The zero-order kinetics of the photoreduction of the Mo_{18}^{6-} ions within both PHEMA and PVA films is in agreement with previous findings relative to the photoreduction of those ions in aqueous solutions of isopropyl alcohol.[7,25] (b) The rate of the $2e^-$ photoreduction is higher than the rate of the $4e^-$ photoreduction within the PHEMA film (2.2 times higher), as resulted from the comparison of the corresponding slopes of the fitting lines (curves A and B; Figure 1c). The same is valid for the PVA film (2.7 times higher; curves C and D, Figure 1c). That result is consistent with literature reporting that the stepwise reduction of the majority of POMs, including the Mo_{18}^{6-} ions, drives the redox potential to more negative values.[7,28] (c) Both the $2e^-$ and $4e^-$ photoreduction rates of the Mo_{18}^{6-} ions within the PVA matrix are higher than the corresponding rates within the PHEMA matrix (3.2 and 2.7 times higher, respectively; Figure 1c), despite the approximately similar Mo_{18}^{6-}/polymer unit molar ratio used in both films. A possible explanation of that finding could be based on the higher stability of the secondary hydroxyalkyl radicals formed in the PVA matrix in relation to the primary hydroxyalkyl radicals formed in the PHEMA matrix.[21] The secondary hydroxyalkyl radicals formed inside the PVA film are possibly further stabilized through their subsequent dehydration,[24] whereas no similar reaction takes place inside the PHEMA film.

b. Monitoring of Mo_{18}^{6-} Photoreduction with FTIR Spectroscopy. The photoreduction of the Mo_{18}^{6-} ions within a PVA film is also followed with FTIR spectroscopy (Figure 2a; Table 1a) in order to further investigate this process. Although it is known that the FTIR band intensity does not always reflect the concentration of local sites, the monitoring of the FTIR bands' intensity of the Mo_{18}^{6-} ions during their photoreduction provides clear indications about the trend of the local sites' change throughout that process. In particular, the P−O_a bonds (where O_a represents the central oxygens of the Dawson structure of the Mo_{18}^{6-} ions; Figure 2a, insets) seem to be dissociated during the photoreduction of those ions, as

(27) Hill, C. L.; Bouchard, D. A. *J. Am. Chem. Soc.* **1985**, *107*, 5148.

(28) Papaconstantinou, E.; Pope, M. T. *Inorg. Chem.* **1967**, *6*, 1152.

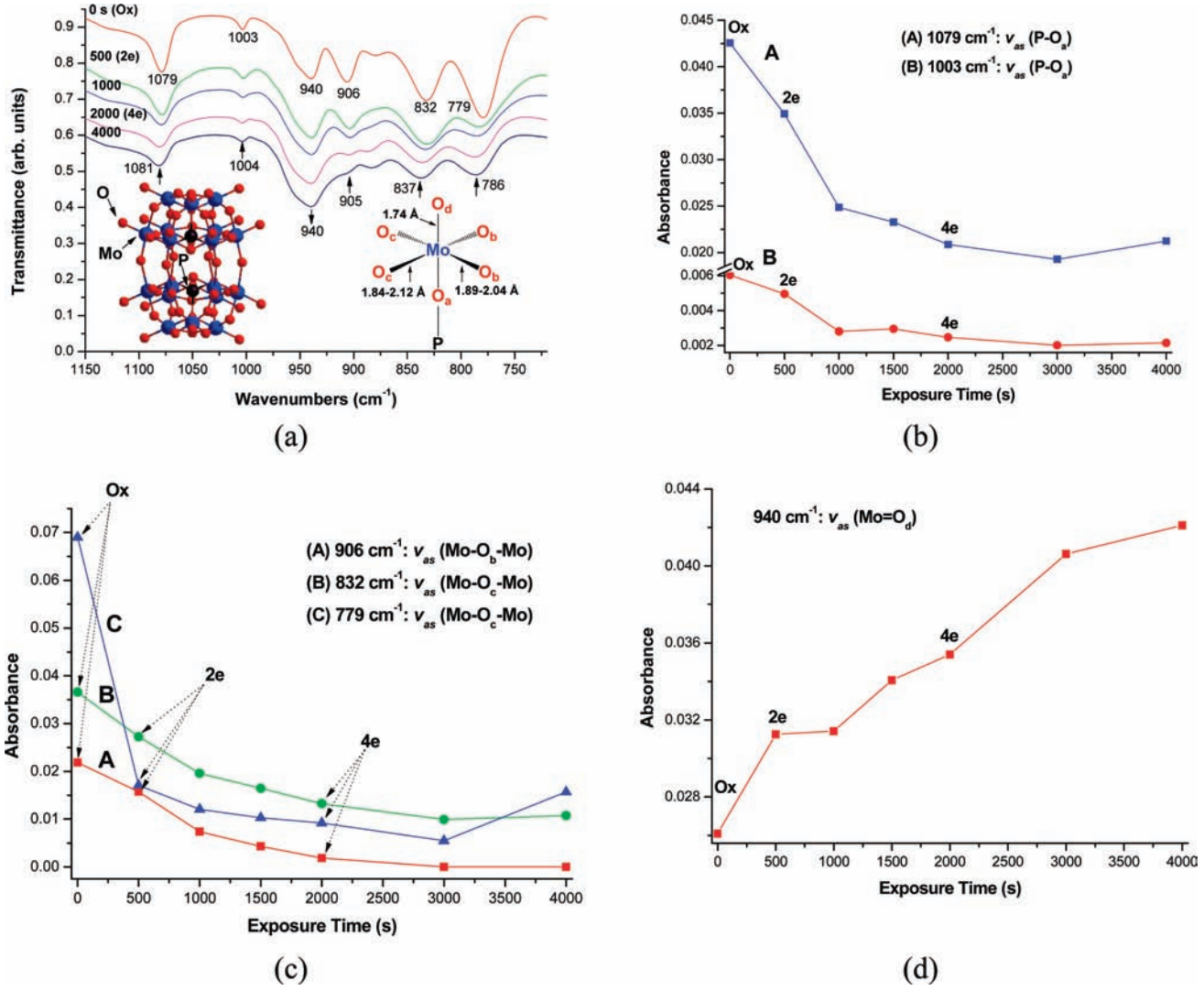

Figure 2. (a) FTIR monitoring of the photoreduction of the Mo_{18}^{6-} ions within a PVA film. The exposure times (s) are indicated on the spectra. Left inset: Representation of the Dawson structure of α-$[P_2Mo_{18}O_{62}]^{6-}$ ion. Right inset: The structure of a MoO_6 octahedron contained in the Dawson structure of α-$[P_2Mo_{18}O_{62}]^{6-}$ ion.[3] (b–d) Change of the FTIR bands' intensity of the Mo_{18}^{6-} ions with the exposure time, within a PVA film. The FTIR bands studied are (b) 1079 and 1003 cm^{-1} (ν_{as} (P−O_a)), (c) 906 cm^{-1} (ν_{as} (Mo−O_b−Mo)), 832 and 779 cm^{-1} (ν_{as} (Mo−O_c−Mo)), and (d) 940 cm^{-1} (ν_{as} (Mo═O_d)). (The process conditions were identical to those in Figure 1b.)

shown from the decrease of the intensity of the asymmetric stretching of the P−O_a bonds (1079 and 1003 cm^{-1}; Figure 2b).[29] The dissociation of the P−O_a bonds during the photoreduction of the Mo_{18}^{6-} ions agrees with a previous experimental finding reporting the reduction of the Keggin-type 12-molybdophosphate ions, $[PMo_{12}O_{40}]^{3-}$, in both the vapor and liquid phase[30] (the Keggin structure is closely related with the Dawson structure giving usually similar redox properties to POMs). In fact, the structural changes of the Mo_{18}^{6-} (and W_{18}^{6-}) ions during their photoreduction appear to be a very interesting topic for a future investigation using complementary techniques (e.g., XPS, electrochemical measurements) in both solution and polymeric films.

The Mo−O_b−Mo bridges (where O_b represents the oxygens that bridge the corner-sharing MoO_6 octahedra, i.e., the oxygens that belong to different Mo_3O_{13} triads) are also dissociated during the photoreduction of the Mo_{18}^{6-} ions, as evidenced by the decrease of the intensity of the asymmetric stretching of the Mo−O_b−Mo bridges (906 cm^{-1}; Figure 2c).[29] Similarly, the Mo−O_c−Mo bridges (where O_c represents the oxygens that bridge the edge-sharing MoO_6 octahedra, i.e., the oxygens that belong to the same Mo_3O_{13} triad) are dissociated throughout the photoreduction of the Mo_{18}^{6-} ions, as shown from the decrease of the intensity of the asymmetric stretching of the Mo−O_c−Mo bridges (832 and 779 cm^{-1}; Figure 2c).[29] The dissociation of the Mo−$O_{b,c}$−Mo bridges during the photoreduction of the Mo_{18}^{6-} ions is also consistent with the aforementioned experimental finding relative to the reduction of the $[PMo_{12}O_{40}]^{3-}$ ions.[30] A possible explanation about the dissociation of the Mo−$O_{b,c}$−Mo bridges during the photoreduction of the Mo_{18}^{6-} ions is that the HOMO and LUMO (highest occupied and lowest unoccupied molecular orbitals, respectively) of the ions are highly composed of the 2p atomic orbitals of the $O_{b,c}$ oxygens

(29) Yang, G.; Gong, J.; Yang, R.; Guo, H.; Wang, Y.; Liu, B.; Dong, S. *Electrochem. Commun.* **2006**, *8*, 790.
(30) Eguchi, K.; Toyozawa, Y.; Yamazoe, N.; Seiyama, T. *J. Catal.* **1983**, *83*, 32.

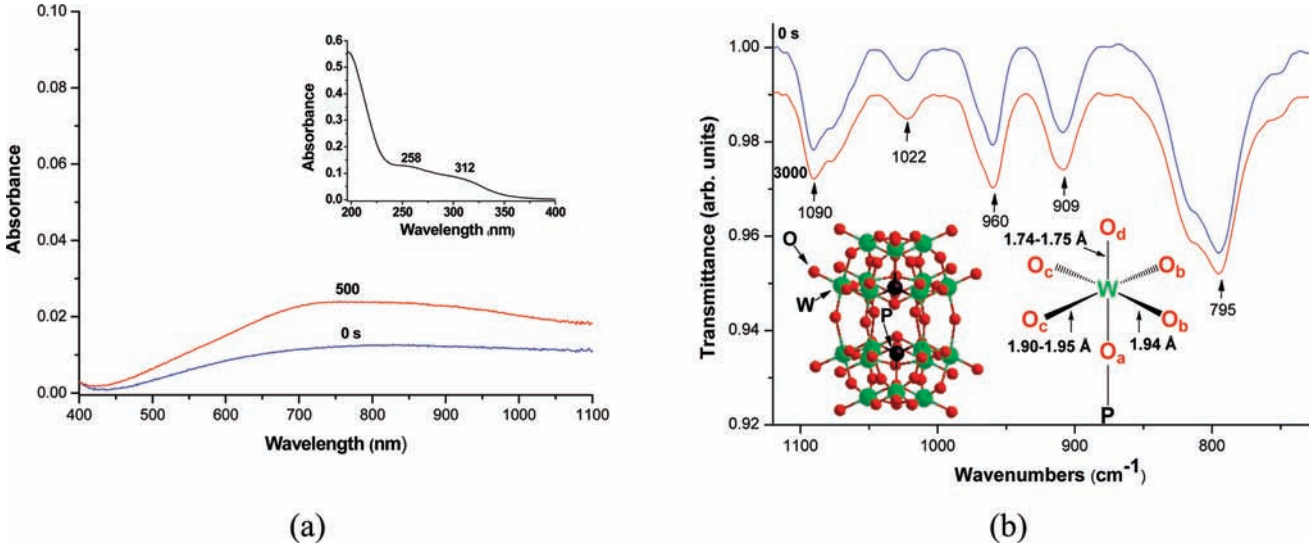

Figure 3. Photoreduction monitoring of the W_{18}^{6-} ions within a PHEMA film. (a) UV spectra showing partial photoreduction of the W_{18}^{6-} ions (e.g., after 500 s exposure) within a PHEMA film. Inset: The initial UV spectrum of the W_{18}^{6-} ions within the PHEMA film. (b) FTIR spectra showing partial photoreduction of the W_{18}^{6-} ions (e.g., after 3000 s irradiation) within the PHEMA film. Left inset: Representation of the Dawson structure of the α-$[P_2W_{18}O_{62}]^{6-}$ ion. Right inset: The structure of a WO_6 octahedron contained in the Dawson structure of the α-$[P_2W_{18}O_{62}]^{6-}$ ion.[3] (The process conditions are described in ref 42.)

(and the corresponding d orbitals of the metal) and that the LUMO is antibonding with respect to the Mo−$O_{b,c}$ bonds. Upon photoreduction of the Mo_{18}^{6-} ions, electrons are added to the LUMO, resulting therefore, in the weakening and, finally, dissociation of the Mo−$O_{b,c}$−Mo bridges. That explanation is in agreement with previous theoretical results obtained for the reduction of the $[PMo_{12}O_{40}]^{3-}$ ions.[31] In addition, a noteworthy observation is that the two kinds of Mo−O_c−Mo bridges are not dissociated to the same degree during the photoreduction of the Mo_{18}^{6-} ions, as shown from the significantly higher decrease of the intensity of the 779 cm^{-1} peak in relation to the intensity of the 832 cm^{-1} peak (Figure 2c). That behavior could be accounted for if the two peaks at 779 and 832 cm^{-1} are attributed to the O_c oxygens that belong to the equatorial (belt) octahedra and polar (cap) octahedra, respectively. This finding is consistent with previous theoretical results reporting that the LUMOs of the equatorial octahedra of the Dawson structure are lower in energy than the LUMOs of their polar octahedra, and therefore the reduction takes place more favorably at the equatorial sites.[3]

On the other hand, the Mo=O_d bonds (where O_d represents the terminal oxygens) seem to be formed during the photoreduction of the Mo_{18}^{6-} ions, as documented by the increase of the intensity of the asymmetric stretching of the Mo=O_d bonds (940 cm^{-1}; Figure 2d).[29] Some irregularities observed in the change of that peak could be ascribed to the broadening of the peak throughout the photoreduction. The formation of the Mo=O_d bonds during the photoreduction of the Mo_{18}^{6-} ions could be possibly explained on the basis of the assumption that the Mo−$O_{b,c}$−Mo bridges dissociated in the photoreduction process (as previously evidenced) form new Mo=O_d bonds, but the whole issue needs further investigation. Similar structural changes have been also detected during the photoreduction of the Mo_{18}^{6-} ions within a PHEMA film (see Supporting Information).

c. Photoreduction of W_{18}^{6-} Ions. In addition to the photoreduction of the Mo_{18}^{6-} ions, the photoreduction of the W_{18}^{6-} ions within PHEMA films is studied with UV and FTIR spectroscopy (Figure 3; Table 1b). It is proved that the W_{18}^{6-} ions are photoreduced within PHEMA films upon broad-band DUV irradiation (220−280 nm) of their OMCT bands (O → W; Figure 3a inset). Nevertheless, only partially photoreduced W_{18}^{6-} ions within PHEMA films are depicted in both UV and FTIR spectra (Figure 3a,b), because, in contrast with the Mo_{18}^{6-} ions, the W_{18}^{6-} ions are rapidly reoxidized by oxygen, requiring, therefore, conditions of complete oxygen absence for the observation of fully photoreduced W_{18}^{6-} ions.[32] Also, the OMCT bands of the W_{18}^{6-} ions embedded within PHEMA films (Figure 3a inset; Table 1b) are shifted (∼13 nm) in relation to the corresponding bands of the ions dissolved in acidified aqueous solutions,[33] as expected from the literature.[27] Small shifts are also observed in the FTIR bands of the W_{18}^{6-} ions (Figure 3b; Table 1b).[34]

d. Discussion of the Photoreduction Mechanism. Having shown that upon UV irradiation both Mo_{18}^{6-} and W_{18}^{6-} ions are photoreduced within PHEMA films, the photoreduction mechanism, for instance, of the W_{18}^{6-} ions (within PHEMA films), could be written as shown in Scheme 1. Initially, the W_{18}^{6-} ions are preassociated with the PHEMA molecules (reaction 1), a result which is subsequently presented during the FTIR study of the films and is in accordance with previous findings.[8] The photoreduction mechanism of Scheme 1 is analogous to that reported in the literature regarding the catalytic photooxidation of alcohols by POMs in solution.[7] A similar reaction mechanism is expected for the photore-

(31) Taketa, H.; Katsuki, S.; Eguchi, K.; Seiyama, T.; Yamazoe, N. *J. Phys. Chem.* **1986**, *90*, 2959.
(32) Argitis, P.; Papaconstantinou, E. *J. Photochem.* **1985**, *30*, 445.
(33) Varga, G. M.; Papaconstaninou, E.; Pope, M. T. *Inorg. Chem.* **1970**, *9*, 662.
(34) Niu, J.; Zhao, J.; Guo, D.; Wang, J. *J. Mol. Struct.* **2004**, *692*, 223.

duction of the Mo_{18}^{6-} ions within PHEMA films, with the only difference being that the photoreduction of those ions proceeds through $2e^-$ addition steps (instead of the $1e^-$ reduction steps of the W_{18}^{6-} ions).[7,25] Also from this mechanism, it is obvious that acid is generated from the photoreduction of both POMs within PHEMA films, an acid which is catalytically regenerated from the following acid-catalyzed cross-linking of PHEMA.[35] The reoxidation of the photoreduced W_{18}^{6-} ions by dioxygen inside the PHEMA films may have a negative impact on the concentration of the photogenenarated acid, because protons and dioxygen are reported to be involved in that reaction.[7,9] Nevertheless, the acid concentration inside the PHEMA films is not expected to decrease considerably, for three major reasons: (a) the acid is catalytically regenerated through PHEMA cross-linking; (b) the generated acid is mainly located in the vicinity of the PHEMA molecules; (c) the presence of dioxygen is rather limited inside the PHEMA films.

2. Acid Generation Monitoring. a. Selection of Acid Indicator. The acid photogenerated by both POMs within PHEMA films could be detected with the addition of a suitable acid indicator. In the present work, DANS has been selected as an acid indicator (Scheme 2), for three basic reasons: (a) The absorption peak of the nonprotonated form of DANS is located at a sufficiently higher wavelength than the OMCT bands of both POMs investigated (i.e., at 445 nm vs 326 nm, respectively; the highest position of the OMCT band of both POMs within PHEMA films is at 326 nm), and therefore the incident irradiation is approximately absorbed only by POM. (b) The major absorption peak of DANS (at 445 nm) gradually vanishes upon its protonation and shifts to a much lower wavelength (345 nm).[19,36] (c) DANS is not photodegradated (through photocatalytic oxidation) by both POMs investigated. In contrast, methylene blue[37] (a dye which also meets the previous two requirements and was initially used as an acid indicator in this work) was photocatalytically destroyed by both Mo_{18}^{6-} and W_{18}^{6-} ions (data not shown), a finding which is in accordance with the photodegradation of the dye by $H_3PW_{12}O_{40}$ recently reported.[38]

Prior to the use of DANS in the acid generation monitoring of both POMs, the protonotion of DANS either by a known PAG or by a solid acid, within PHEMA films, was studied. In the first case, the protonation of DANS induced by the photoacid generation of a known PAG (triphenylsulfonium hexafluoroantimonate, TPSHFA) within a PHEMA film was studied with UV spectroscopy (Figure 4a). In this case, the acid generated through the 254 nm irradiation of TPSHFA induces protonation of DANS, as evidenced by (a) the gradual disappearance of the 446 nm absorption peak of DANS, with the exposure time, and (b) the appearance of

Scheme 1. Mechanism of Photoacid Generation by the W_{18}^{6-} Ions within PHEMA Films

$$W_{18}^{6-} + RCH_2CH_2OH \rightleftharpoons (W_{18}^{6-}\ RCH_2CH_2OH) \quad (1)$$

$$(W_{18}^{6-}\ RCH_2CH_2OH) \overset{h\nu}{\rightleftharpoons} ({}^*W_{18}^{6-}\ RCH_2CH_2OH) \quad (2)$$

$$({}^*W_{18}^{6-}\ RCH_2CH_2OH) \longrightarrow W_{18}^{7-} + RCH_2\dot{C}HOH + H^+ \quad (3)$$

$$W_{18}^{7-} + RCH_2\dot{C}HOH \longrightarrow W_{18}^{8-} + RCH_2CHO + H^+ \quad (4)$$

$$W_{18}^{6-} + RCH_2\dot{C}HOH \longrightarrow W_{18}^{7-} + RCH_2CHO + H^+ \quad (5)$$

$$W_{18}^{8-} + W_{18}^{6-} \longrightarrow 2W_{18}^{7-} \quad (6)$$

R =

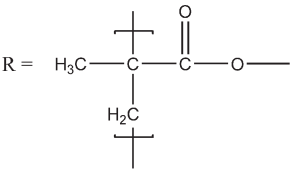

Scheme 2. DANS Protonation

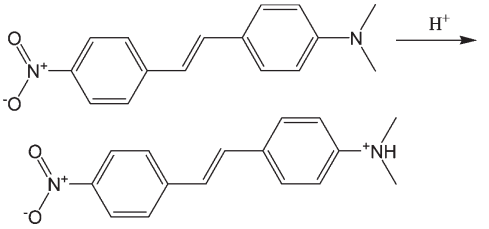

a shoulder at ~346 nm attributed to the protonated form of DANS. The difficulty of distinguishing the peak of the protonated form of DANS at ~346 nm probably stems from the high film thickness of the PHEMA films that is necessary in the present work in order to avoid DANS removal from the films during spin-coating (see Experimental Section). In the second case, the protonation of DANS caused by the gradual addition of a solid acid (i.e., the heteropoly acid $H_3PW_{12}O_{40}$), within a PHEMA film is studied with UV spectroscopy (Figure 4b). Similar spectral changes of DANS are observed in this case as well, indicating clearly that DANS is protonated by the addition of the solid acid.

b. Acid Generation Monitoring with Indicator. DANS is introduced in PHEMA films of both POMs investigated, and its protonation upon POM photoreduction is followed with UV spectroscopy (Figure 4c,d). Using deep UV (254 nm) irradiation, the Mo_{18}^{6-} ions indeed generate acid within a PHEMA film (Figure 4c), as documented by the gradual decrease of the major absorption peak of DANS (at 448 nm) with the exposure time, and the appearance of the peak of the protonated DANS (at 343 nm). These spectral changes are similar to those previously encountered with both the TPSHFA and $H_3PW_{12}O_{40}$, and also to those in the literature.[19,36] The spectra in Figure 4c correspond exclusively to DANS, because the spectra of the Mo_{18}^{6-} ions have been subtracted from them. In particular, the spectra of the Mo_{18}^{6-} − PHEMA film have been subtracted from the spectra of the Mo_{18}^{6-}−DANS−PHEMA film, where both films were prepared and processed under identical conditions. This was done because the 343 nm peak of the protonated

(35) (a) Vasilopoulou, M.; Boyatzis, S.; Raptis, I.; Dimotikalli, D.; Argitis, P. *J. Mater. Chem.* **2004**, *14*, 3312. (b) Lee, J.; Aoai, T.; Kondo, S.; Miyagawa, N.; Takahara, S.; Yamaoka, T. *J. Polym. Sci., Part A* **2002**, *40*, 1858.

(36) Georgiadou, D. G.; Vasilopoulou, M.; Pistolis, G.; Palilis, L.; Dimotikali, D.; Argitis, P. *Phys. Status Solidi A* **2008**, *205*, 2526.

(37) (a) Kiwi, J.; Denisov, N.; Nadtochenko, V. *J Phys. Chem. B* **1999**, *103*, 9141. (b) Bergmann, K.; O'Konski, C. T. *J. Phys. Chem.* **1963**, *67*, 2169.

(38) Yang, Y.; Wu, Q.; Guo, Y.; Hu, C.; Wang, E. *J. Mol. Catal. A* **2005**, *225*, 203.

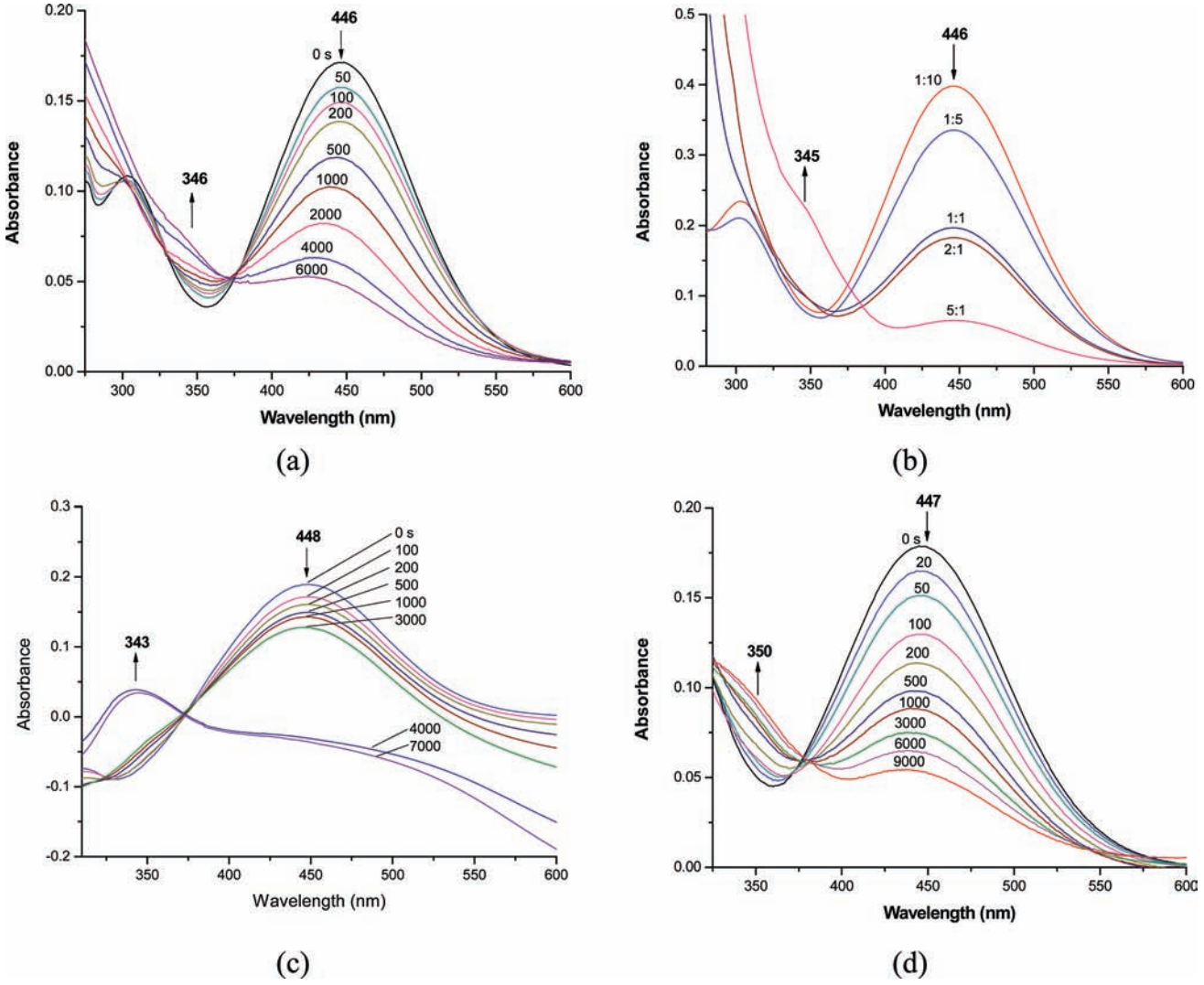

Figure 4. UV monitoring of the DANS protonation (within PHEMA films) induced by (a) the photoacid generation of a known PAG (TPSHFA), (b) the addition of a solid acid ($H_3PW_{12}O_{40}$), (c) the photoacid generation of the Mo_{18}^{6-} ions, and (d) the photoacid generation of the W_{18}^{6-} ions. In a, c, and d, the exposure times (s) are indicated on the spectra, whereas in b, the molar ratios $H_3PW_{12}O_{40}$/DANS are shown on the spectra. In c, the UV spectra are resulted from the subtraction of spectra of the Mo_{18}^{6-}−PHEMA film from the Mo_{18}^{6-}−DANS−PHEMA film (both films were prepared and processed under identical conditions). Similarly, in d, the UV spectra are resulted from the subtraction of spectra of the W_{18}^{6-}−PHEMA film from the W_{18}^{6-}−DANS−PHEMA film (both films were prepared and processed under the same conditions). (The process conditions are described in ref 43.)

DANS had been completely covered by the large shoulder of the Mo_{18}^{6-} ions at ~320 nm, in the Mo_{18}^{6-}−DANS−PHEMA film (see the Supporting Information). It should be noticed that the subtraction of the UV spectra is not perfect, due to small differences in film thickness, and thus, a few irregularities are observed in the UV spectra sequence of Figure 4c.

The W_{18}^{6-} ions are also found to generate acid upon 254 nm irradiation, within a PHEMA film (Figure 4d). The subtraction of spectra (the W_{18}^{6-}−DANS−PHEMA film minus the W_{18}^{6-}−PHEMA film, both prepared and processed under the same conditions) was also necessary in the case of the W_{18}^{6-} ions, because the peak of the protonated DANS (at ~350 nm) was covered by the large shoulder of the W_{18}^{6-} ions (at ~320 nm) in the W_{18}^{6-}−DANS−PHEMA film (see the Supporting Information). Spectral changes of DANS similar to those encountered with the Mo_{18}^{6-} ions support the photoacid generation of the W_{18}^{6-} ions with the only difference being that a shoulder (instead of a clear peak) at ~350 nm is obtained for the protonated form of DANS. Obviously, this resulted, as in the case of Mo_{18}^{6-}, from the fact that the subtraction of the corresponding spectra of W_{18}^{6-} is not perfect.

3. Acid-Catalyzed Cross-Linking of PHEMA. a. Imaging Experiments. It is known that PHEMA is catalytically cross-linked in the presence of acid, mainly via a transesterification mechanism.[35] For the investigation of the acid-catalyzed cross-linking of PHEMA films by the two investigated POMs, a photolithographic process comprising a series of three steps (i.e., UV irradiation, PEB, and development in pure water; see the Experimental Section) was followed. In that process, the acid generated by POMs upon UV exposure catalyzes the cross-linking of the PHEMA film throughout the PEB step. When the PHEMA film is adequately cross-linked, it becomes insoluble in water used as developer during the following development step (the unexposed POM-containing PHEMA film is soluble in water, due to the high solubility of POMs in water). Having the above consid-

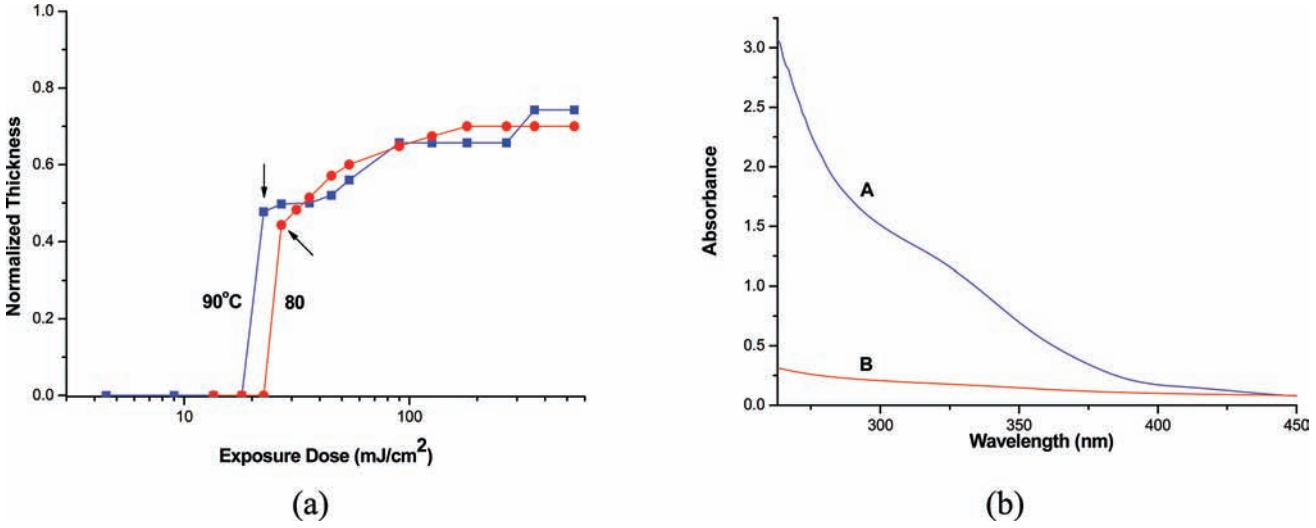

Figure 5. Study of the imaging behavior of the Mo_{18}^{6-}−PHEMA films. (a) Contrast curves of two Mo_{18}^{6-}−PHEMA films showing the effect of the exposure dose and PEB temperature on the normalized film thickness. The doses necessary for the PHEMA cross-linking are indicated. (b) UV spectra showing the effect of the development in pure water on a photo-cross-linked Mo_{18}^{6-}−PHEMA film (curve A, prior to the development; curve B, after the development). (The process conditions are described in ref 44.)

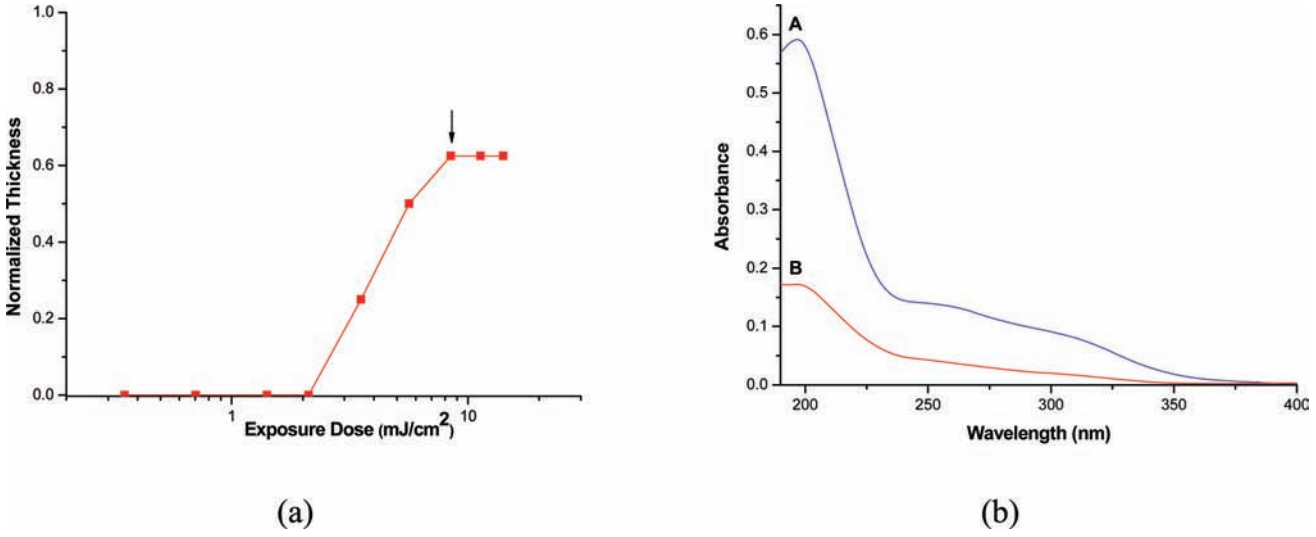

Figure 6. Study of the imaging behavior of the W_{18}^{6-}−PHEMA films. (a) Contrast curve of the W_{18}^{6-}−PHEMA film showing the effect of the exposure dose on the normalized film thickness. The dose necessary for the PHEMA cross-linking is indicated. (b) UV spectra showing the effect of the development in pure water on a photo-cross-linked W_{18}^{6-}−PHEMA film (curve A, before the development; curve B, after the development). (The process conditions are described in ref 45.)

erations in mind, the effect of the exposure dose and PEB temperature on the thickness of the Mo_{18}^{6-}−PHEMA film at the end of the photolithographic process divided by the initial film thickness (normalized thickness) is studied (Figure 5a). As shown in that figure, upon an increase of the PEB temperature (Figure 5a), the necessary (for the PHEMA cross-linking) exposure dose decreases, and therefore, the photosensitivity of the film increases.[18] That behavior is a classical behavior of a negative tone photoresist and is analogous to the PHEMA cross-linking by known photoacid generators.[35] A point that needs to be stressed is that a significant loss (~40%) of film thickness takes place during the development of the film in pure water. This is caused by the washing of the Mo_{18}^{6-} ions from the film throughout the development, as shown from the corresponding UV spectra (Figure 5b). That result was expected, because it has been reported that POMs are also leached from PVA-based resist films during the development of the films with water, if acids or salts are not added in the developer solution.[24] Nevertheless, in the present investigation, we chose to work with water (except for a limited number of cases where ethyl lactate was used) as a developer and examine the possibility of PHEMA cross-linking and removing all of the POMs from the film at the end of the process.

Similar results are also obtained from the investigation of the imaging behavior of the W_{18}^{6-}−PHEMA film. Thus, from the study of the effect of the exposure dose on the normalized film thickness (at a constant PEB temperature; Figure 6a), the PHEMA photo-cross-linking is achieved at a specific exposure dose or higher (a dose that characterizes the photosensitivity of the film). By comparing the necessary (for the PHEMA cross-linking) exposure doses of the two films, Mo_{18}^{6-}−PHEMA

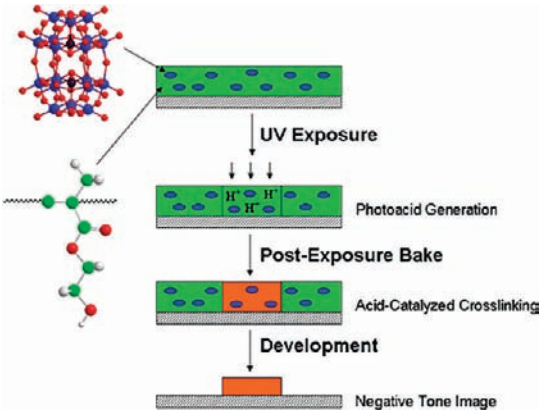

Figure 7. Schematic representation of the photolithographic process followed for the acid-catalyzed cross-linking of PHEMA by the investigated POMs.

and W_{18}^{6-}−PHEMA (22.5 vs 8.5 mJ/cm^2; Figure 5a (PEB 90 °C) and Figure 6a, respectively), it is evident that the latter film is more photosensitive than the former. This finding is further supported by the fact that more favorable photolithographic conditions were applied in the first film than in the second film, that is, a higher concentration of the Mo_{18}^{6-} ions in comparison with the W_{18}^{6-} ions and broad-band DUV (220−280 nm) irradiation of the Mo_{18}^{6-}−PHEMA film versus the 248 nm exposure of the W_{18}^{6-}−PHEMA film. Consequently, the W_{18}^{6-} ions are more efficient at inducing acid-catalyzed cross-linking of PHEMA and, therefore, more efficient in photoacid generation, than the Mo_{18}^{6-} ions. The latter finding is consistent with previous studies reporting that the W_{18}^{6-} ions are more effective photooxidizing reagents than the Mo_{18}^{6-} ions in solution, due to their fast reoxidation by oxygen.[7,9] Furthermore, a considerable loss (∼40%) of film thickness occurs in this case during the development of the film in pure water, due to washing of the W_{18}^{6-} ions from the film (Figure 6b). The leaching of the W_{18}^{6-} ions from the PHEMA film takes place in a way similar to that of the Mo_{18}^{6-} ions previously discussed.[24]

From the above imaging study, it is evident that the photolithographic scheme followed in the acid-catalyzed cross-linking of PHEMA by POMs is analogous to the scheme employed in the acid-catalyzed cross-linking of chemically amplified resists (Figure 7). The difference in the process applied here is that the developer used can be pure water, and the photoacid generator (POM) is removed from the polymer films during the development. Applying that photolithographic scheme in POM-containing PHEMA films, some characteristic imaging results of the films are obtained (Figure 8). The best resolution (herein, the minimum line width) achieved is 0.5 μm for the Mo_{18}^{6-}−PHEMA film and 1 μm for the W_{18}^{6-}−PHEMA film (both at 2:1 lines/spaces, l/s; Figure 8a,c, respectively). Better-quality images are obtained at a higher dimension, 1.5 μm for both the Mo_{18}^{6-}−PHEMA and the W_{18}^{6-}−PHEMA films (2:1 l/s; Figure 8b,d, respectively), but still the image contrast is low. The images of the Mo_{18}^{6-}−PHEMA film (Figure 8a,b) were obtained by using ethyl lactate as a developer in the photolithographic process.

b. Spectroscopic Monitoring of PHEMA Changes during Processing. The chemical changes in PHEMA functionalities during the imaging of the POM-containing PHEMA films were investigated with FTIR spectroscopy (Figure 9) in order to better characterize the cross-linking process. From the FTIR study of the Mo_{18}^{6-}−PHEMA film (Figure 9a), three major findings are concluded: (a) The Mo_{18}^{6-} ions are preassociated with the PHEMA matrix through intermolecular hydrogen bonding (reaction 1). This is mainly documented by the huge split of the O−H stretching peak of PHEMA into two peaks (3439 → 3502, 3224 cm^{-1}) and also from the large shift of the C=O stretching peak to lower wavenumbers (1728 → 1716 cm^{-1}; curves A and B, Figure 9a).[39] The preassociation of the Mo_{18}^{6-} ions with the PHEMA matrix is consistent with literature reporting that the catalytic photooxidation of an organic compound by POM in solution proceeds through preassociation of the POM with the organic compound.[8] A similar experimental finding is also obtained when the Mo_{18}^{6-} ions are embedded in

(39) (a) Bertoluzza, A.; Monti, P.; Garcia-Ramos, J. V.; Simoni, R.; Caramazza, R.; Calzavara, A. *J. Mol. Struct.* **1986**, *143*, 469. (b) Lipschitz, I. *Polym. Plast. Technol. Eng.* **1982**, *19*, 53. (c) Matsura, H.; Hiraishi, M.; Miyazawa, T. *Spectrochim. Acta* **1972**, *28A*, 2299.

(40) The process conditions in Table 1 were as follows: (a) Mo_{18}^{6-}−PHEMA, 53.4−6.28% (w/w EL); PAB, 90 °C, 5 min; exposure, 220−280 nm. Mo_{18}^{6-}−PVA, 76.6−4.4% (w/w aq.); PAB, 75 °C, 2 min; exposure, 220−280 nm. Incident power, 0.18 mW/cm^2. (b) For the UV: W_{18}^{6-}−PHEMA, 40.4−4.71% (w/w MeOH/H_2O, weight ratio 1.3:1). For the FTIR: W_{18}^{6-}−PHEMA, 40.4−4.46% (w/w MeOH/H_2O, weight ratio 1.1:1).

(41) The process conditions in Figure 1 were as follows. (a) Solution: Mo_{18}^{6-}−PHEMA, 53.4−6.28% (w/w EL). Process: PAB, 90 °C, 5 min; exposure, 220−280 nm. (b) Solution: Mo_{18}^{6-}−PVA, 76.6−4.4% (w/w aq.). Process: PAB, 75 °C, 2 min; exposure, 220−280 nm. Incident power, 0.18 mW/cm^2.

(42) The process conditions in Figure 3 were as follows: (a) W_{18}^{6-}−PHEMA, 40.4−4.71% (w/w MeOH/H_2O, weight ratio 1.3:1); PAB, 75 °C, 2 min; exposure, 220−280 nm, 500 s. (b) W_{18}^{6-}−PHEMA, 40.4−4.46% (w/w MeOH/H_2O, weight ratio 1.1:1); PAB, 90 °C, 5 min; exposure, 220−280 nm, 3000 s. Incident power, 0.18 mW/cm^2.

(43) The process conditions in Figure 4 were as follows: (a) TPSHFA−DANS−PHEMA, 0.13−0.07−30% (w/w DMF); molar ratio TPSHFA/DANS, 1:1; PAB, 50 °C, 10 min; exposure through 254 nm broadband filter; incident power, 6.949 × 10^{-3} mW/cm^2. (b) Solutions of DANS−PHEMA 0.07−30% (w/w DMF) containing different molar ratios of $H_3PW_{12}O_{40}$/DANS ranging from 1:10 to 5:1 were used; PAB, 50 °C, 10 min. (c) Two solutions were used: Mo_{18}^{6-}−DANS−PHEMA, 1.18−0.11−30% (w/w DMF), molar ratio Mo_{18}^{6-}/DANS, 1:1; Mo_{18}^{6-}−PHEMA, 1.18−30% (w/w DMF). PAB, 50 °C, 10 min; exposure through 254 nm broadband filter; incident power, 6.694 × 10^{-3} mW/cm^2. (d) Two solutions were used: W_{18}^{6-}−DANS−PHEMA, 1.18−0.07−30% (w/w DMF), molar ratio W_{18}^{6-}/DANS, 1:1; W_{18}^{6-}−PHEMA, 1.18−30% (w/w DMF). PAB, 50 °C, 10 min; exposure through 254 nm broadband filter; incident power, 7.204 × 10^{-3} mW/cm^2.

(44) The process conditions in Figure 5 were as follows: (a) Mo_{18}^{6-}−PHEMA, 53.4−6.28% (w/w EL). PAB, 75 °C, 2 min; exposure, 220−280 nm; PEB, 80/90 °C, 2 min; development in pure water, 15 s; film thickness after PAB, 350 nm. (b) Mo_{18}^{6-}−PHEMA, 75.2−6.28% (w/w EL). Curve A: PAB, 90 °C, 5 min; exposure, 220−280 nm, 3000 s; PEB, 90 °C, 5 min. Curve B: The same process with curve A, but with one additional step: development in pure water, 15 s. Film thickness after PAB, 513 nm; film thickness after development, 200 nm.

(45) The process conditions in Figure 6 were as follows: (a) W_{18}^{6-}−PHEMA, 40.4−3.51% (w/w MeOH/H_2O weight ratio, 0.7:1); PAB, 75 °C, 2 min; exposure at 248 nm; PEB, 90 °C, 2 min; development in pure water, 15 s; film thickness after PAB, 120 nm. (b) W_{18}^{6-}−PHEMA, 40.4−4.71% (w/w in MeOH/H_2O weight ratio, 1.3:1). Curve A: PAB, 75 °C, 2 min; exposure, 220−280 nm, 4000 s; PEB, 90 °C, 5 min. Curve B: The same process as with curve A, but with one additional step: development in pure water, 15 s.

(46) The process conditions in Figure 8 were as follows: (a,b) Mo_{18}^{6-}−PHEMA, 53.4−6.28% (w/w EL); PAB, 75 °C, 2 min; exposure, 248 nm, 4000 s; PEB, 80 °C, 2 min; development in EL, 1 min. (c, d) W_{18}^{6-}−PHEMA, 40.4−3.66% (w/w MeOH/H_2O weight ratio, 0.8:1); PAB, 75 °C, 2 min; exposure, 248 nm, 3000 s; PEB, 90 °C, 2 min; development in pure water, 15 s.

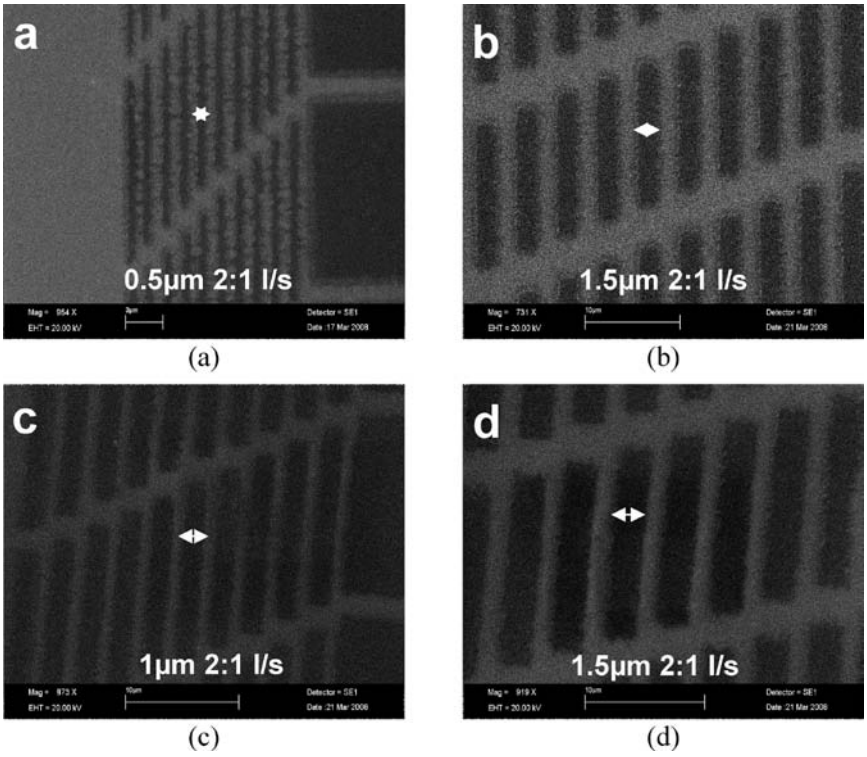

Figure 8. SEM micrographs of the images obtained by the UV photolithographic processing of two films: (a,b) Mo_{18}^{6-}−PHEMA film and (c,d) W_{18}^{6-}−PHEMA film. (The process conditions are described in ref 46.)

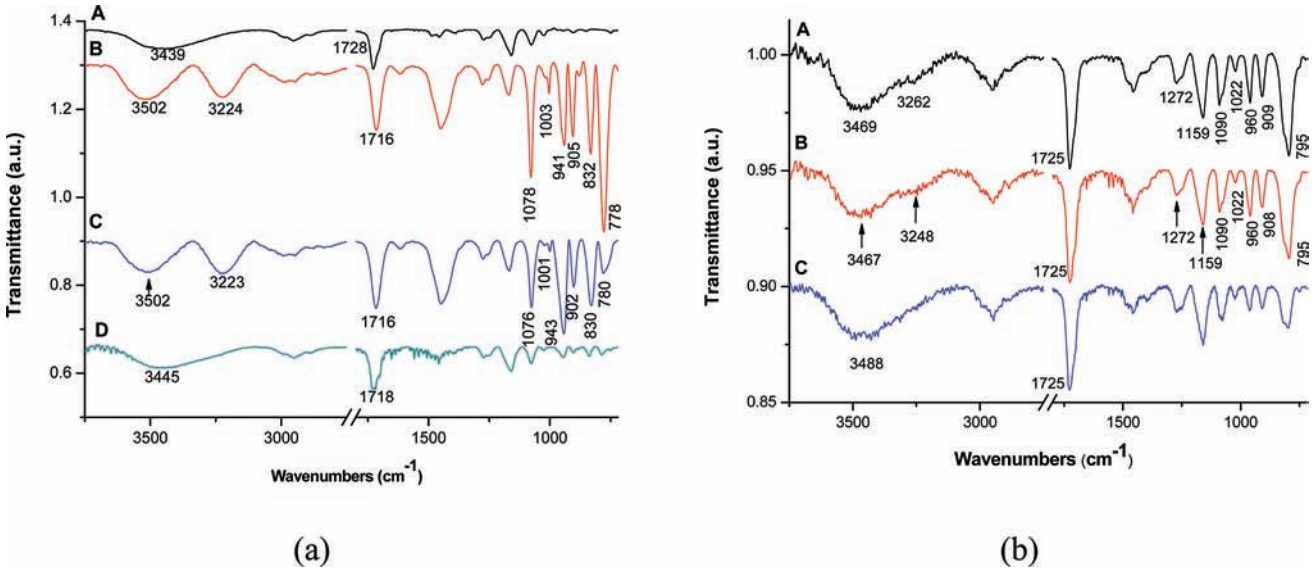

Figure 9. FTIR spectra showing the chemical changes in PHEMA functionalities: (a) in a Mo_{18}^{6-}−PHEMA film and (b) in a W_{18}^{6-}−PHEMA film. (a) Curve A, a PHEMA film; curve B, the initial (not photo-cross-linked) Mo_{18}^{6-}−PHEMA film; curve C, the photo-cross-linked Mo_{18}^{6-}−PHEMA film; curve D, the Mo_{18}^{6-}−PHEMA film after the development in pure water. (b) Curve A, the initial (not photo-cross-linked) W_{18}^{6-}−PHEMA film; curve B, the photo-cross-linked W_{18}^{6-}−PHEMA film; curve C, the W_{18}^{6-}−PHEMA film after the development in pure water. (The process conditions are described in ref 47.)

(47) The process conditions in Figure 9 were as follows. (a) Curve A: PHEMA, 6.28% (w/w EL); PAB, 80 °C, 5 min. Curves B−D: Mo_{18}^{6-}−PHEMA, 75.2−6.28% (w/w EL). Curve B: PAB, 90 °C, 5 min. Curve C: The same process as with curve B, but with two additional steps: exposure, 220−280 nm, 3000 s; PEB, 90 °C, 5 min. Curve D: The same process as with curve C plus development in pure water, 15 s. Film thickness after PAB, 513 nm; film thickness after development, 200 nm. (b) W_{18}^{6-}−PHEMA, 40.4−4.46% (w/w MeOH/H_2O weight ratio, 1.1:1). Curve A: PAB, 90 °C, 5 min. Curve B: The same process as with curve A, plus exposure, 220−280 nm, 3000 s; PEB, 90 °C, 5 min. Curve C: The same process as with curve B, plus development in pure water, 15 s.

the PVA matrix (see the Supporting Information). (b) Small chemical changes are induced by the acid-catalyzed cross-linking of PHEMA. In particular, the PHEMA cross-linking by the photogenerated acid is documented only by a small decrease in the intensity of the O−H stretching peak of PHEMA (at 3502 cm^{-1}; curve C, Figure 9a). That result is expected, because it has been reported that, although the acid-catalyzed cross-linking of PHEMA brings about a huge decrease of PHEMA solubility in polar solvents, the induced chemical changes

in PHEMA functionalities are very small and hardly detectable with FTIR spectroscopy.[35] (c) The Mo_{18}^{6-} ions are removed during the development of the PHEMA films in pure water, as shown from the dramatic decrease of the FTIR peaks of the ions (1076−780 cm^{-1}; curves C and D, Figure 9a). It is noticeable that, after the removal of the Mo_{18}^{6-} ions from the PHEMA films, the O−H stretching peak is reestablished at one peak coming back almost to its initial position (3445 cm^{-1}; curve D, Figure 9a). That is a further proof of the hydrogen bonding between Mo_{18}^{6-} ions and PHEMA matrix.

Similar results are also obtained from the FTIR study of the W_{18}^{6-}−PHEMA film (Figure 9b): (a) The W_{18}^{6-} ions are also preassociated with the PHEMA matrix through hydrogen bonding, as shown from the split of the O−H stretching peak of PHEMA into two peaks (3439 → 3469, 3262 cm^{-1}; curves A of Figures 9a,b). Nevertheless, in this case, the preassociation takes place to a lower degree than with the Mo_{18}^{6-} ions, as the split of the O−H peak is inferior. This is probably due to the lower concentration of the W_{18}^{6-} ions in relation to the Mo_{18}^{6-} ions. (b) Small chemical changes are also induced by the acid-catalyzed cross-linking of PHEMA. That result is supported by the following changes in the intensities of the FTIR peaks of PHEMA: a small decrease in the intensity of the O−H stretching peak of PHEMA (3467 cm^{-1}); a small decrease in the intensity of the peak ascribed to the wagging of CH_2, rocking of CH_2, and asymmetric stretching of the CC(=O)O group (1272 cm^{-1}); and a small decrease in the intensity of the peak attributed to the asymmetric stretching of the C−O−C group (1159 cm^{-1}; curve B, Figure 9b).[39] (c) The W_{18}^{6-} ions are removed during the development of the PHEMA films in pure water, as shown from the decrease of the FTIR peaks of the ions (1090−795 cm^{-1}; curves B and C, Figure 9b). After the removal of the W_{18}^{6-} ions, the O−H stretching peak is restored at one peak (3488 cm^{-1}; curve C, Figure 9b), just as previously met with the Mo_{18}^{6-} ions, though to a lower degree.

Conclusions

In the present work, it is demonstrated that both Mo_{18}^{6-} and W_{18}^{6-} ions photochemically generate acid within films of a polymer that includes hydroxylic functional groups, that is, within PHEMA films. The acid is generated from the simultaneous photoreduction of POM and oxidation of PHEMA, whereas it is regenerated during the subsequent acid-catalyzed cross-linking of PHEMA. The photoreduction of both POMs within PHEMA films (and supportively within PVA films) is monitored with UV and FTIR spectroscopy. Significant findings concerning mainly the Mo_{18}^{6-} ions are extracted from this study: (a) both the $2e^-$ and $4e^-$ photoreductions of the Mo_{18}^{6-} ions follow zero-order kinetics, and (b) the $P-O_a$ bonds and the $Mo-O_{b,c}-Mo$ bridges of the Mo_{18}^{6-} ions are dissociated during the photoreduction of the ions, whereas the $Mo=O_d$ bonds are formed. Furthermore, the photoacid generation efficiency of both POMs within PHEMA films is evidenced with the addition of an appropriate acid indicator (DANS) and following its protonation with UV spectroscopy. From the comparison of the efficiency of both POMs to induce acid-catalyzed cross-linking of PHEMA under similar photolithographic conditions, the W_{18}^{6-} ion is found to be more efficient photoacid generator than the Mo_{18}^{6-} ion. Characteristic imaging results of ~1 μm resolution are obtained from the photolithographic processing of the POM-containing PHEMA films. In that process, both POMs can be almost entirely washed away from the PHEMA films during the development with pure water, resulting therefore in patterned (POM-free) PHEMA films. Conclusively, both POMs investigated are suitable photoacid generators for the patterning of PHEMA films through acid-catalyzed cross-linking, providing also an interesting characteristic when compared to common photoacid generators: they are washed away from the films during the development. The whole photoacid generation behavior of the investigated POMs is expected to find application in areas such as in patterning of biomaterials, including not only PHEMA but other polymers with hydroxylic functionalities as well. Applications in proton transporting systems are also envisioned.

Supporting Information Available: FTIR monitoring of Mo_{18}^{6-} ions within PHEMA films, UV spectra of the Mo_{18}^{6-}−DANS−PHEMA and W_{18}^{6-}−DANS−PHEMA films (without subtraction of the spectra of the Mo_{18}^{6-} and W_{18}^{6-} ions, respectively), preassociation of Mo_{18}^{6-} ions with PVA matrix. This material is available free of charge via the Internet at http://pubs.acs.org.